Search for the semileptonic decay $D_s^+ \to \pi^0 e^+ \nu_e$

M. Ablikim,[1] M. N. Achasov,[10,b] P. Adlarson,[67] M. Albrecht,[4] R. Aliberti,[28] A. Amoroso,[66a,66c] M. R. An,[32] Q. An,[63,50] X. H. Bai,[58] Y. Bai,[49] O. Bakina,[29] R. Baldini Ferroli,[23a] I. Balossino,[24a] Y. Ban,[39,g] V. Batozskaya,[1,37] D. Becker,[28] K. Begzsuren,[26] N. Berger,[28] M. Bertani,[23a] D. Bettoni,[24a] F. Bianchi,[66a,66c] J. Bloms,[60] A. Bortone,[66a,66c] I. Boyko,[29] R. A. Briere,[5] A. Brueggemann,[60] H. Cai,[68] X. Cai,[1,50] A. Calcaterra,[23a] G. F. Cao,[1,55] N. Cao,[1,55] S. A. Cetin,[54a] J. F. Chang,[1,50] W. L. Chang,[1,55] G. Chelkov,[29,a] C. Chen,[36] Chao Chen,[47] G. Chen,[1] H. S. Chen,[1,55] M. L. Chen,[1,50] S. J. Chen,[35] S. M. Chen,[53] T. Chen,[1] X. R. Chen,[25,55] X. T. Chen,[1] Y. B. Chen,[1,50] Z. J. Chen,[20,h] W. S. Cheng,[66c] X. Chu,[36] G. Cibinetto,[24a] F. Cossio,[66c] J. J. Cui,[42] H. L. Dai,[1,50] J. P. Dai,[70] A. Dbeyssi,[14] R. E. de Boer,[4] D. Dedovich,[29] Z. Y. Deng,[1] A. Denig,[28] I. Denysenko,[29] M. Destefanis,[66a,66c] F. De Mori,[66a,66c] Y. Ding,[33] J. Dong,[1,50] L. Y. Dong,[1,55] M. Y. Dong,[1,50,55] X. Dong,[68] S. X. Du,[72] P. Egorov,[29,a] Y. L. Fan,[68] J. Fang,[1,50] S. S. Fang,[1,55] W. X. Fang,[1] Y. Fang,[1] R. Farinelli,[24a] L. Fava,[66b,66c] F. Feldbauer,[4] G. Felici,[23a] C. Q. Feng,[63,50] J. H. Feng,[51] K. Fischer,[61] M. Fritsch,[4] C. Fritzsch,[60] C. D. Fu,[1] H. Gao,[55] Y. N. Gao,[39,g] Yang Gao,[63,50] S. Garbolino,[66c] I. Garzia,[24a,24b] P. T. Ge,[68] Z. W. Ge,[35] C. Geng,[51] E. M. Gersabeck,[59] A. Gilman,[61] K. Goetzen,[11] L. Gong,[33] W. X. Gong,[1,50] W. Gradl,[28] M. Greco,[66a,66c] L. M. Gu,[35] M. H. Gu,[1,50] C. Y. Guan,[1,55] A. Q. Guo,[25,55] L. B. Guo,[34] R. P. Guo,[41] Y. P. Guo,[9,f] A. Guskov,[29,a] T. T. Han,[42] W. Y. Han,[32] X. Q. Hao,[15] F. A. Harris,[57] K. K. He,[47] K. L. He,[1,55] F. H. Heinsius,[4] C. H. Heinz,[28] Y. K. Heng,[1,50,55] C. Herold,[52] M. Himmelreich,[11,d] G. Y. Hou,[1,55] Y. R. Hou,[55] Z. L. Hou,[1] H. M. Hu,[1,55] J. F. Hu,[48,i] T. Hu,[1,50,55] Y. Hu,[1] G. S. Huang,[63,50] K. X. Huang,[51] L. Q. Huang,[25,55] L. Q. Huang,[64] X. T. Huang,[42] Y. P. Huang,[1] Z. Huang,[39,g] T. Hussain,[65] N. Hüsken,[22,28] W. Imoehl,[22] M. Irshad,[63,50] J. Jackson,[22] S. Jaeger,[4] S. Janchiv,[26] Q. Ji,[1] Q. P. Ji,[15] X. B. Ji,[1,55] X. L. Ji,[1,50] Y. Y. Ji,[42] Z. K. Jia,[63,50] H. B. Jiang,[42] S. S. Jiang,[32] X. S. Jiang,[1,50,55] Y. Jiang,[55] J. B. Jiao,[42] Z. Jiao,[18] S. Jin,[35] Y. Jin,[58] M. Q. Jing,[1,55] T. Johansson,[67] N. Kalantar-Nayestanaki,[56] X. S. Kang,[33] R. Kappert,[56] M. Kavatsyuk,[56] B. C. Ke,[72] I. K. Keshk,[4] A. Khoukaz,[60] P. Kiese,[28] R. Kiuchi,[1] R. Kliemt,[11] L. Koch,[30] O. B. Kolcu,[54a] B. Kopf,[4] M. Kuemmel,[4] M. Kuessner,[4] A. Kupsc,[37,67] W. Kühn,[30] J. J. Lane,[59] J. S. Lange,[30] P. Larin,[14] A. Lavania,[21] L. Lavezzi,[66a,66c] Z. H. Lei,[63,50] H. Leithoff,[28] M. Lellmann,[28] T. Lenz,[28] C. Li,[36] C. Li,[40] C. H. Li,[32] Cheng Li,[63,50] D. M. Li,[72] F. Li,[1,50] G. Li,[1] H. Li,[44] H. Li,[63,50] H. B. Li,[1,55] H. J. Li,[15] H. N. Li,[48,i] J. Q. Li,[4] J. S. Li,[51] J. W. Li,[42] Ke Li,[1] L. J. Li,[1] L. K. Li,[1] Lei Li,[3] M. H. Li,[36] P. R. Li,[31,j,k] S. X. Li,[9] S. Y. Li,[53] T. Li,[42] W. D. Li,[1,55] W. G. Li,[1] X. H. Li,[63,50] X. L. Li,[42] Xiaoyu Li,[1,55] Z. Y. Li,[51] H. Liang,[63,50] H. Liang,[27] H. Liang,[1,55] Y. F. Liang,[46] Y. T. Liang,[25,55] G. R. Liao,[12] L. Z. Liao,[42] J. Libby,[21] A. Limphirat,[52] C. X. Lin,[51] D. X. Lin,[25,55] T. Lin,[1] B. J. Liu,[1] C. X. Liu,[1] D. Liu,[14,63] F. H. Liu,[45] Fang Liu,[1] Feng Liu,[6] G. M. Liu,[48,i] H. Liu,[31,j,k] H. M. Liu,[1,55] Huanhuan Liu,[1] Huihui Liu,[16] J. B. Liu,[63,50] J. L. Liu,[64] J. Y. Liu,[1,55] K. Liu,[1] K. Y. Liu,[33] Ke Liu,[17] L. Liu,[63,50] M. H. Liu,[9,f] P. L. Liu,[1] Q. Liu,[55] S. B. Liu,[63,50] T. Liu,[9,f] W. K. Liu,[36] W. M. Liu,[63,50] X. Liu,[31,j,k] Y. Liu,[31,j,k] Y. B. Liu,[36] Z. A. Liu,[1,50,55] Z. Q. Liu,[42] X. C. Lou,[1,50,55] F. X. Lu,[51] H. J. Lu,[18] J. G. Lu,[1,50] X. L. Lu,[1] Y. Lu,[1] Y. P. Lu,[1,50] Z. H. Lu,[1] C. L. Luo,[34] M. X. Luo,[71] T. Luo,[9,f] X. L. Luo,[1,50] X. R. Lyu,[55] Y. F. Lyu,[36] F. C. Ma,[33] H. L. Ma,[1] L. L. Ma,[42] M. M. Ma,[1,55] Q. M. Ma,[1] R. Q. Ma,[1,55] R. T. Ma,[55] X. Y. Ma,[1,50] Y. Ma,[39,g] F. E. Maas,[14] M. Maggiora,[66a,66c] S. Maldaner,[4] S. Malde,[61] Q. A. Malik,[65] A. Mangoni,[23b] Y. J. Mao,[39,g] Z. P. Mao,[1] S. Marcello,[66a,66c] Z. X. Meng,[58] J. G. Messchendorp,[56,11] G. Mezzadri,[24a] H. Miao,[1] T. J. Min,[35] R. E. Mitchell,[22] X. H. Mo,[1,50,55] N. Yu. Muchnoi,[10,b] Y. Nefedov,[29] I. B. Nikolaev,[10,b] Z. Ning,[1,50] S. Nisar,[8,l] Y. Niu,[42] S. L. Olsen,[55] Q. Ouyang,[1,50,55] S. Pacetti,[23b,23c] X. Pan,[9,f] Y. Pan,[49] A. Pathak,[1] A. Pathak,[27] M. Pelizaeus,[4] H. P. Peng,[63,50] K. Peters,[11,d] J. Pettersson,[67] J. L. Ping,[34] R. G. Ping,[1,55] S. Plura,[28] S. Pogodin,[29] V. Prasad,[63,50] F. Z. Qi,[1] H. Qi,[63,50] H. R. Qi,[53] M. Qi,[35] T. Y. Qi,[9,f] S. Qian,[1,50] W. B. Qian,[55] Z. Qian,[51] C. F. Qiao,[55] J. J. Qin,[64] L. Q. Qin,[12] X. P. Qin,[9,f] X. S. Qin,[42] Z. H. Qin,[1,50] J. F. Qiu,[1] S. Q. Qu,[36] S. Q. Qu,[53] K. H. Rashid,[65] C. F. Redmer,[28] K. J. Ren,[32] A. Rivetti,[66c] V. Rodin,[56] M. Rolo,[66c] G. Rong,[1,55] Ch. Rosner,[14] S. N. Ruan,[36] H. S. Sang,[63] A. Sarantsev,[29,c] Y. Schelhaas,[28] C. Schnier,[4] K. Schoenning,[67] M. Scodeggio,[24a,24b] K. Y. Shan,[9,f] W. Shan,[19] X. Y. Shan,[63,50] J. F. Shangguan,[47] L. G. Shao,[1,55] M. Shao,[63,50] C. P. Shen,[9,f] H. F. Shen,[1,55] X. Y. Shen,[1,55] B.-A. Shi,[55] H. C. Shi,[63,50] J. Y. Shi,[1] q. q. Shi,[47] R. S. Shi,[1,55] X. Shi,[1,50] X. D. Shi,[63,50] J. J. Song,[15] W. M. Song,[27,1] Y. X. Song,[39,g] S. Sosio,[66a,66c] S. Spataro,[66a,66c] F. Stieler,[28] K. X. Su,[68] P. P. Su,[47] Y.-J. Su,[55] G. X. Sun,[1] H. Sun,[55] H. K. Sun,[1] J. F. Sun,[15] L. Sun,[68] S. S. Sun,[1,55] T. Sun,[1,55] W. Y. Sun,[27] X. Sun,[20,h] Y. J. Sun,[63,50] Y. Z. Sun,[1] Z. T. Sun,[42] Y. H. Tan,[68] Y. X. Tan,[63,50] C. J. Tang,[46] G. Y. Tang,[1] J. Tang,[51] L. Y. Tao,[64] Q. T. Tao,[20,h] M. Tat,[61] J. X. Teng,[63,50] V. Thoren,[67] W. H. Tian,[44] Y. Tian,[25,55] I. Uman,[54b] B. Wang,[1] B. L. Wang,[55] C. W. Wang,[35] D. Y. Wang,[39,g] F. Wang,[64] H. J. Wang,[31,j,k] H. P. Wang,[1,55] K. Wang,[1,50] L. L. Wang,[1] M. Wang,[42] M. Z. Wang,[39,g] Meng Wang,[1,55] S. Wang,[9,f] T. Wang,[9,f] T. J. Wang,[36] W. Wang,[51] W. H. Wang,[68] W. P. Wang,[63,50] X. Wang,[39,g] X. F. Wang,[31,j,k] X. L. Wang,[9,f] Y. D. Wang,[38] Y. F. Wang,[1,50,55] Y. H. Wang,[40] Y. Q. Wang,[1] Yi Wang,[53] Ying Wang,[51] Z. Wang,[1,50] Z. Y. Wang,[1,55] Ziyi Wang,[55] D. H. Wei,[12] F. Weidner,[60] S. P. Wen,[1] D. J. White,[59] U. Wiedner,[4] G. Wilkinson,[61] M. Wolke,[67] L. Wollenberg,[4] J. F. Wu,[1,55] L. H. Wu,[1] L. J. Wu,[1,55] X. Wu,[9,f] X. H. Wu,[27] Y. Wu,[63] Z. Wu,[1,50] L. Xia,[63,50] T. Xiang,[39,g] D. Xiao,[31,j,k] G. Y. Xiao,[35] H. Xiao,[9,f] S. Y. Xiao,[1] Y. L. Xiao,[9,f] Z. J. Xiao,[34] C. Xie,[35] X. H. Xie,[39,g] Y. Xie,[42] Y. G. Xie,[1,50] Y. H. Xie,[6] Z. P. Xie,[63,50] T. Y. Xing,[1,55] C. F. Xu,[1] C. J. Xu,[51]

G. F. Xu,[1] H. Y. Xu,[58] Q. J. Xu,[13] S. Y. Xu,[62] X. P. Xu,[47] Y. C. Xu,[55] Z. P. Xu,[35] F. Yan,[9,f] L. Yan,[9,f] W. B. Yan,[63,50] W. C. Yan,[72] H. J. Yang,[43,e] H. L. Yang,[27] H. X. Yang,[1] L. Yang,[44] S. L. Yang,[55] Tao Yang,[1] Y. X. Yang,[1,55] Yifan Yang,[1,55] M. Ye,[1,50] M. H. Ye,[7] J. H. Yin,[1] Z. Y. You,[51] B. X. Yu,[1,50,55] C. X. Yu,[36] G. Yu,[1,55] T. Yu,[64] C. Z. Yuan,[1,55] L. Yuan,[2] S. C. Yuan,[1] X. Q. Yuan,[1] Y. Yuan,[1,55] Z. Y. Yuan,[51] C. X. Yue,[32] A. A. Zafar,[65] F. R. Zeng,[42] X. Zeng,[6] Y. Zeng,[20,h] Y. H. Zhan,[51] A. Q. Zhang,[1] B. L. Zhang,[1] B. X. Zhang,[1] D. H. Zhang,[36] G. Y. Zhang,[15] H. Zhang,[63] H. H. Zhang,[27] H. H. Zhang,[51] H. Y. Zhang,[1,50] J. L. Zhang,[69] J. Q. Zhang,[34] J. W. Zhang,[1,50,55] J. X. Zhang,[31,j,k] J. Y. Zhang,[1] J. Z. Zhang,[1,55] Jianyu Zhang,[1,55] Jiawei Zhang,[1,55] L. M. Zhang,[53] L. Q. Zhang,[51] Lei Zhang,[35] P. Zhang,[1] Q. Y. Zhang,[32,72] Shulei Zhang,[20,h] X. D. Zhang,[38] X. M. Zhang,[1] X. Y. Zhang,[47] X. Y. Zhang,[42] Y. Zhang,[61] Y. T. Zhang,[72] Y. H. Zhang,[1,50] Yan Zhang,[63,50] Yao Zhang,[1] Z. H. Zhang,[1] Z. Y. Zhang,[36] Z. Y. Zhang,[68] G. Zhao,[1] J. Zhao,[32] J. Y. Zhao,[1,55] J. Z. Zhao,[1,50] Lei Zhao,[63,50] Ling Zhao,[1] M. G. Zhao,[36] Q. Zhao,[1] S. J. Zhao,[72] Y. B. Zhao,[1,50] Y. X. Zhao,[25,55] Z. G. Zhao,[63,50] A. Zhemchugov,[29,a] B. Zheng,[64] J. P. Zheng,[1,50] Y. H. Zheng,[55] B. Zhong,[34] C. Zhong,[64] X. Zhong,[51] H. Zhou,[42] L. P. Zhou,[1,55] X. Zhou,[68] X. K. Zhou,[55] X. R. Zhou,[63,50] X. Y. Zhou,[32] Y. Z. Zhou,[9,f] J. Zhu,[36] K. Zhu,[1] K. J. Zhu,[1,50,55] L. X. Zhu,[55] S. H. Zhu,[62] S. Q. Zhu,[35] T. J. Zhu,[69] W. J. Zhu,[9,f] Y. C. Zhu,[63,50] Z. A. Zhu,[1,55] B. S. Zou,[1] and J. H. Zou[1]

(BESIII Collaboration)

[1]*Institute of High Energy Physics, Beijing 100049, People's Republic of China*
[2]*Beihang University, Beijing 100191, People's Republic of China*
[3]*Beijing Institute of Petrochemical Technology, Beijing 102617, People's Republic of China*
[4]*Bochum Ruhr-University, D-44780 Bochum, Germany*
[5]*Carnegie Mellon University, Pittsburgh, Pennsylvania 15213, USA*
[6]*Central China Normal University, Wuhan 430079, People's Republic of China*
[7]*China Center of Advanced Science and Technology, Beijing 100190, People's Republic of China*
[8]*COMSATS University Islamabad, Lahore Campus, Defence Road, Off Raiwind Road, 54000 Lahore, Pakistan*
[9]*Fudan University, Shanghai 200433, People's Republic of China*
[10]*G.I. Budker Institute of Nuclear Physics SB RAS (BINP), Novosibirsk 630090, Russia*
[11]*GSI Helmholtzcentre for Heavy Ion Research GmbH, D-64291 Darmstadt, Germany*
[12]*Guangxi Normal University, Guilin 541004, People's Republic of China*
[13]*Hangzhou Normal University, Hangzhou 310036, People's Republic of China*
[14]*Helmholtz Institute Mainz, Staudinger Weg 18, D-55099 Mainz, Germany*
[15]*Henan Normal University, Xinxiang 453007, People's Republic of China*
[16]*Henan University of Science and Technology, Luoyang 471003, People's Republic of China*
[17]*Henan University of Technology, Zhengzhou 450001, People's Republic of China*
[18]*Huangshan College, Huangshan 245000, People's Republic of China*
[19]*Hunan Normal University, Changsha 410081, People's Republic of China*
[20]*Hunan University, Changsha 410082, People's Republic of China*
[21]*Indian Institute of Technology Madras, Chennai 600036, India*
[22]*Indiana University, Bloomington, Indiana 47405, USA*
[23a]*INFN Laboratori Nazionali di Frascati, I-00044 Frascati, Italy*
[23b]*INFN Sezione di Perugia, I-06100 Perugia, Italy*
[23c]*University of Perugia, I-06100 Perugia, Italy*
[24a]*INFN Sezione di Ferrara, I-44122 Ferrara, Italy*
[24b]*University of Ferrara, I-44122 Ferrara, Italy*
[25]*Institute of Modern Physics, Lanzhou 730000, People's Republic of China*
[26]*Institute of Physics and Technology, Peace Ave. 54B, Ulaanbaatar 13330, Mongolia*
[27]*Jilin University, Changchun 130012, People's Republic of China*
[28]*Johannes Gutenberg University of Mainz, Johann-Joachim-Becher-Weg 45, D-55099 Mainz, Germany*
[29]*Joint Institute for Nuclear Research, 141980 Dubna, Moscow region, Russia*
[30]*Justus-Liebig-Universitaet Giessen, II. Physikalisches Institut, Heinrich-Buff-Ring 16, D-35392 Giessen, Germany*
[31]*Lanzhou University, Lanzhou 730000, People's Republic of China*
[32]*Liaoning Normal University, Dalian 116029, People's Republic of China*
[33]*Liaoning University, Shenyang 110036, People's Republic of China*
[34]*Nanjing Normal University, Nanjing 210023, People's Republic of China*
[35]*Nanjing University, Nanjing 210093, People's Republic of China*
[36]*Nankai University, Tianjin 300071, People's Republic of China*
[37]*National Centre for Nuclear Research, Warsaw 02-093, Poland*
[38]*North China Electric Power University, Beijing 102206, People's Republic of China*

[39]*Peking University, Beijing 100871, People's Republic of China*
[40]*Qufu Normal University, Qufu 273165, People's Republic of China*
[41]*Shandong Normal University, Jinan 250014, People's Republic of China*
[42]*Shandong University, Jinan 250100, People's Republic of China*
[43]*Shanghai Jiao Tong University, Shanghai 200240, People's Republic of China*
[44]*Shanxi Normal University, Linfen 041004, People's Republic of China*
[45]*Shanxi University, Taiyuan 030006, People's Republic of China*
[46]*Sichuan University, Chengdu 610064, People's Republic of China*
[47]*Soochow University, Suzhou 215006, People's Republic of China*
[48]*South China Normal University, Guangzhou 510006, People's Republic of China*
[49]*Southeast University, Nanjing 211100, People's Republic of China*
[50]*State Key Laboratory of Particle Detection and Electronics, Beijing 100049, Hefei 230026, People's Republic of China*
[51]*Sun Yat-Sen University, Guangzhou 510275, People's Republic of China*
[52]*Suranaree University of Technology, University Avenue 111, Nakhon Ratchasima 30000, Thailand*
[53]*Tsinghua University, Beijing 100084, People's Republic of China*
[54a]*Turkish Accelerator Center Particle Factory Group, Istinye University, 34010 Istanbul, Turkey*
[54b]*Near East University, Nicosia, North Cyprus, Mersin 10, Turkey*
[55]*University of Chinese Academy of Sciences, Beijing 100049, People's Republic of China*
[56]*University of Groningen, NL-9747 AA Groningen, The Netherlands*
[57]*University of Hawaii, Honolulu, Hawaii 96822, USA*
[58]*University of Jinan, Jinan 250022, People's Republic of China*
[59]*University of Manchester, Oxford Road, Manchester M13 9PL, United Kingdom*
[60]*University of Muenster, Wilhelm-Klemm-Str. 9, 48149 Muenster, Germany*
[61]*University of Oxford, Keble Rd, Oxford OX13RH, United Kingdom*
[62]*University of Science and Technology Liaoning, Anshan 114051, People's Republic of China*
[63]*University of Science and Technology of China, Hefei 230026, People's Republic of China*
[64]*University of South China, Hengyang 421001, People's Republic of China*
[65]*University of the Punjab, Lahore-54590, Pakistan*
[66a]*University of Turin, I-10125 Turin, Italy*
[66b]*University of Eastern Piedmont, I-15121 Alessandria, Italy*
[66c]*INFN, I-10125 Turin, Italy*
[67]*Uppsala University, Box 516, SE-75120 Uppsala, Sweden*
[68]*Wuhan University, Wuhan 430072, People's Republic of China*
[69]*Xinyang Normal University, Xinyang 464000, People's Republic of China*
[70]*Yunnan University, Kunming 650500, People's Republic of China*
[71]*Zhejiang University, Hangzhou 310027, People's Republic of China*
[72]*Zhengzhou University, Zhengzhou 450001, People's Republic of China*

(Received 28 June 2022; accepted 31 October 2022; published 12 December 2022)

[a]Also at the Moscow Institute of Physics and Technology, Moscow 141700, Russia.
[b]Also at the Novosibirsk State University, Novosibirsk 630090, Russia.
[c]Also at the NRC "Kurchatov Institute," PNPI, 188300 Gatchina, Russia.
[d]Also at Goethe University Frankfurt, 60323 Frankfurt am Main, Germany.
[e]Also at Key Laboratory for Particle Physics, Astrophysics and Cosmology, Ministry of Education; Shanghai Key Laboratory for Particle Physics and Cosmology; Institute of Nuclear and Particle Physics, Shanghai 200240, People's Republic of China.
[f]Also at Key Laboratory of Nuclear Physics and Ion-beam Application (MOE) and Institute of Modern Physics, Fudan University, Shanghai 200443, People's Republic of China.
[g]Also at State Key Laboratory of Nuclear Physics and Technology, Peking University, Beijing 100871, People's Republic of China.
[h]Also at School of Physics and Electronics, Hunan University, Changsha 410082, China.
[i]Also at Guangdong Provincial Key Laboratory of Nuclear Science, Institute of Quantum Matter, South China Normal University, Guangzhou 510006, China.
[j]Also at Frontiers Science Center for Rare Isotopes, Lanzhou University, Lanzhou 730000, People's Republic of China.
[k]Also at Lanzhou Center for Theoretical Physics, Lanzhou University, Lanzhou 730000, People's Republic of China.
[l]Also at the Department of Mathematical Sciences, IBA, Karachi, Pakistan.

We present the first search for the semileptonic decay $D_s^+ \to \pi^0 e^+ \nu_e$ using a data sample of electron-positron collisions recorded with the BESIII detector at center-of-mass energies between 4.178 and 4.226 GeV, corresponding to an integrated luminosity of 6.32 fb^{-1}. This decay is expected to be sensitive to π^0–η mixing. No significant signal is observed. We set an upper limit of 6.4×10^{-5} on the branching fraction at the 90% confidence level.

DOI: 10.1103/PhysRevD.106.112004

I. INTRODUCTION

Neutral mesons that have hidden flavors and the same quantum numbers can mix via the strong and electromagnetic interactions. Meson mixing is an interesting phenomenon that can be used to explain some specific decay processes of heavy mesons. Many mixing effects are being widely studied, such as in the systems $\pi^0 - \eta$ [1], $\rho - \omega$ [2], $\omega - \phi$ [3], and $\eta - \eta'$ [4]. This analysis searches for $\pi^0 - \eta$ mixing in semileptonic D_s^+ decays. The semileptonic decay $D_s^+ \to \pi^0 e^+ \nu_e$ can only occur via $\pi^0 - \eta$ mixing, as shown in Fig. 1, and nonperturbative weak annihilation effects, as shown in Fig. 2, where the two gluons can be emitted from the c quark or $\bar{s}$ quark or one gluon from each quark [1]. However, the radiation of a π^0 from the weak annihilation effect is suppressed not only by the Okubo-Zweig-Iizuka (OZI) rule but also by isospin conservation. Consequently, the weak annihilation contribution to the $D_s^+ \to \pi^0 e^+ \nu_e$ decay is relatively small compared to that from $\pi^0 - \eta$ mixing. The contribution to the branching fraction (BF) of $D_s^+ \to \pi^0 e^+ \nu_e$ from the weak annihilation effect is expected to be only of the order of $10^{-7} - 10^{-8}$, while the contribution from $\pi^0 - \eta$ mixing is expected to be $(2.65 \pm 0.38) \times 10^{-5}$ [1]. Therefore, this decay provides an excellent opportunity to study the $\pi^0 - \eta$ mixing effect.

In this paper, we present the first search for the semileptonic decay $D_s^+ \to \pi^0 e^+ \nu_e$ in a data sample corresponding to an integrated luminosity of 6.32 fb^{-1}, which was recorded by the BESIII detector at center-of-mass (CM) energies ($\sqrt{s}$) between 4.178 and 4.226 GeV. A blind analysis is performed to avoid possible bias. The signal region of the data sample is only uncovered after the event selection and analysis strategy are studied and verified based on an ensemble of forty inclusive MC samples with the same size as the data sample. Throughout this paper, charge conjugate channels are implied.

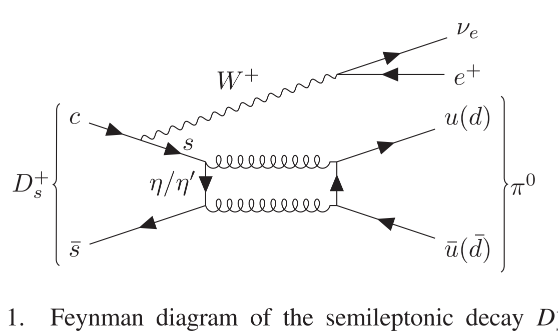

FIG. 1. Feynman diagram of the semileptonic decay $D_s^+ \to \pi^0 e^+ \nu_e$ through $\pi^0 - \eta$ mixing.

II. DETECTOR AND DATASETS

The BESIII detector [5,6] records symmetric e^+e^- collisions provided by the BEPCII storage ring [7], which operates in the CM energy range from 2.0 to 4.9 GeV. The cylindrical core of the BESIII detector covers 93% of the full solid angle and consists of a helium-based multilayer drift chamber (MDC), a plastic scintillator time-of-flight system (TOF), and a CsI(Tl) electromagnetic calorimeter (EMC), which are all enclosed in a superconducting solenoidal magnet providing a 1.0 T magnetic field. The solenoid is supported by an octagonal flux-return yoke with resistive plate counter muon identification modules interleaved with steel. The charged-particle momentum resolution at 1 GeV/c is 0.5%, and the specific energy loss ($\mathrm{d}E/\mathrm{d}x$) resolution is 6% for electrons from Bhabha scattering. The EMC measures photon energies with a

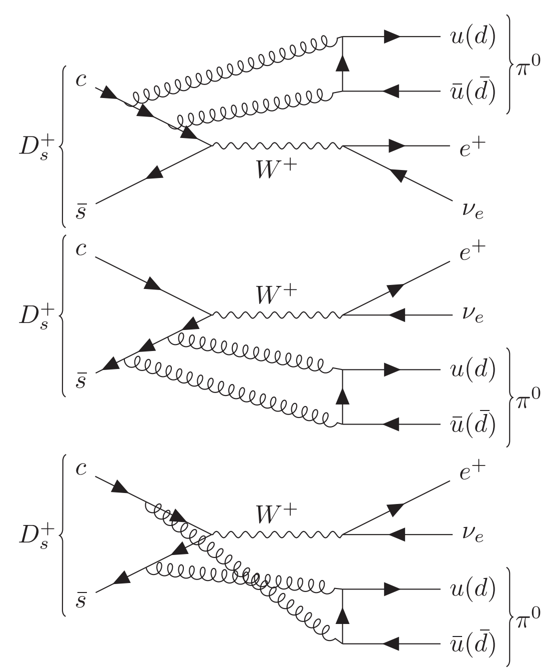

FIG. 2. Feynman diagrams of the semileptonic decay $D_s^+ \to \pi^0 e^+ \nu_e$ through the weak annihilation effect with the radiation of a π^0 meson.

TABLE I. Integrated luminosity $\mathcal{L}_{\rm int}$ and the recoil mass $M_{\rm rec}$ requirements for various energies, where $M_{\rm rec}$ is defined in Eq. (5). The first and second uncertainties are statistical and systematic, respectively. The data collected at $\sqrt{s} = 4.178$–4.219 GeV (which corresponds to about 83.3% of total data sample) use the updated TOF [11,12].

$\sqrt{s}$ (GeV)	$\mathcal{L}_{\rm int}$ (pb^{-1})	$M_{\rm rec}$ (GeV$/c^2$)
4.178	$3189.0 \pm 0.2 \pm 31.9$	[2.050, 2.180]
4.189	$526.7 \pm 0.1 \pm 2.2$	[2.048, 2.190]
4.199	$526.0 \pm 0.1 \pm 2.1$	[2.046, 2.200]
4.209	$517.1 \pm 0.1 \pm 1.8$	[2.044, 2.210]
4.219	$514.6 \pm 0.1 \pm 1.8$	[2.042, 2.220]
4.226	$1056.4 \pm 0.1 \pm 7.0$	[2.040, 2.220]

resolution of 2.5% (5%) at 1 GeV in the barrel (end cap) region. The time resolution in the TOF barrel region is 68 ps, while that in the end cap region is 110 ps. The end cap TOF system was upgraded in 2015 using multigap resistive plate chamber technology, providing a time resolution of 60 ps [8].

The data samples used in this analysis correspond to an integrated luminosity ($\mathcal{L}_{\rm int}$) of 6.32 fb^{-1} taken in the range of $\sqrt{s} = 4.178$ to 4.226 GeV, as listed in Table I. All data samples except the 4.226 GeV one benefit from the improved time resolution in the end caps. In these energies, $D_s^{*\pm}D_s^{\mp}$ events provide a large sample of $D_s^{\pm}$ mesons. The cross section of $D_s^{*\pm}D_s^{\mp}$ production in e^+e^- annihilation is about a factor of 20 larger than that of $D_s^+D_s^-$ [9], and $D_s^{*\pm}$ decays to $\gamma D_s^{\pm}$ with a dominant BF of $(93.5 \pm 0.7)\%$ [10]. Therefore, we use $D_s^{*\pm}D_s^{\mp} \to \gamma D_s^+ D_s^-$ events in this analysis.

Large samples of Monte Carlo (MC) simulated events produced with GEANT4-based [13] software, which includes the geometric description of the BESIII detector and the detector response, are used to determine the detection efficiency and to estimate the background contributions. The simulation includes the beam-energy spread and initial-state radiation (ISR) in the e^+e^- annihilation modeled with the generator KKMC [14]. Inclusive MC samples with 40 times the size of data are used to simulate the background contributions. The inclusive MC samples, which contain no signal $D_s^+ \to \pi^0 e^+\nu_e$ decays, include the production of open-charm processes, the ISR production of vector charmonium(like) states, and the continuum processes incorporated in KKMC. The known decay modes are modeled with EVTGEN [15] using world averaged BF values [10], and the remaining unknown decays from the charmonium states with LUNDCHARM [16]. Final-state radiation from charged final-state particles is incorporated with PHOTOS [17]. The signal detection efficiencies and signal shapes are obtained from signal MC samples, in which the signal $D_s^+ \to \pi^0 e^+\nu_e$ decay is simulated using the ISGW2 model [18,19].

III. DATA ANALYSIS

The process $e^+e^- \to D_s^{*+}D_s^- + \text{c.c.} \to \gamma D_s^+ D_s^-$ allows the study of semileptonic D_s^+ decays with a tag technique [20] since only one neutrino escapes undetected. There are two types of samples used in the tag technique: single tag (ST) and double tag (DT) events. In the ST sample, a D_s^- meson is reconstructed through a specific hadronic decay without any requirement on the remaining measured tracks and EMC showers. In the DT sample, a D_s^-, designated as the "tag," is reconstructed through a hadronic decay mode first, and then the decay $D_s^+ \to \pi^0 e^+\nu_e$, designated as the "signal," is reconstructed with the remaining tracks and EMC showers. For a specific tag mode, the ST yield is given by

$$N_{\rm tag}^{\rm ST} = 2N_{D_s^*D_s}\mathcal{B}_{\rm tag}\epsilon_{\rm tag}^{\rm ST}, \tag{1}$$

and the DT yield is given by

$$N_{\rm tag,sig}^{\rm DT} = 2N_{D_s^*D_s}\mathcal{B}_{\gamma}\mathcal{B}_{\pi^0}\mathcal{B}_{\rm tag}\mathcal{B}_{\rm sig}\epsilon_{\rm tag,sig}^{\rm DT}, \tag{2}$$

where $N_{D_s^*D_s}$ is the total number of $D_s^{*+}D_s^- + \text{c.c.}$ pairs produced, $\mathcal{B}_{\rm sig(tag)}$ is the BF of the signal decay (the tag mode), $\mathcal{B}_{\gamma(\pi^0)}$ is the BF of $D_s^* \to \gamma D_s$ ($\pi^0 \to \gamma\gamma$), and $\epsilon_{\rm tag}^{\rm ST}$ ($\epsilon_{\rm tag,sig}^{\rm DT}$) is the corresponding ST (DT) efficiency. By isolating $\mathcal{B}_{\rm sig}$, one obtains

$$\mathcal{B}_{\rm sig} = \frac{N_{\rm tag,sig}^{\rm DT}\epsilon_{\rm tag}^{\rm ST}}{\mathcal{B}_{\gamma}\mathcal{B}_{\pi^0}N_{\rm tag}^{\rm ST}\epsilon_{\rm tag,sig}^{\rm DT}}, \tag{3}$$

where the yields $N_{\rm tag}^{\rm ST}$ and $N_{\rm tag,sig}^{\rm DT}$ are obtained from data samples, while $\epsilon_{\rm tag}^{\rm ST}$ and $\epsilon_{\rm tag,sig}^{\rm DT}$ are obtained from inclusive and signal MC samples, respectively. For multiple tag modes and energy points, the above equation is generalized as

$$\mathcal{B}_{\rm sig} = \frac{N_{\rm total,sig}^{\rm DT}}{\mathcal{B}_{\gamma}\mathcal{B}_{\pi^0}\sum_{\alpha,i}N_{\alpha,i}^{\rm ST}\epsilon_{\alpha,{\rm sig},i}^{\rm DT}/\epsilon_{\alpha,i}^{\rm ST}}, \tag{4}$$

where α represents tag modes, i represents different energy points, and $N_{\rm total,sig}^{\rm DT}$ is the total signal yield.

The tag candidates are reconstructed with $K^{\pm}$, $\pi^{\pm}$, π^0, ρ^0, η, η', and K_S^0 mesons that satisfy the particle selection criteria detailed below. Twelve tag modes are used, and the requirements on the invariant masses of tagged D_s^- candidates ($M_{\rm tag}$) are summarized in Table II.

Photon candidates are reconstructed from isolated clusters found in the EMC. The EMC shower time is required to be within [0, 700] ns from the event start time in order to suppress fake photons due to electronic noise or e^+e^- beam background. Photon candidates within $|\cos\theta| < 0.80$ (barrel) are required to deposit more than 25 MeV of energy,

TABLE II. Requirements on $M_{\rm tag}$, the ST yields ($N_{\rm tag}^{\rm ST}$) and ST efficiencies ($\epsilon_{\rm tag}^{\rm ST}$) at $\sqrt{s}$ = (I) 4.178 GeV, (II) 4.189–4.219 GeV, and (III) 4.226 GeV, where the subscripts of η and η' denote the decay modes used to reconstruct η and η' candidates. The efficiencies for the energy points 4.189–4.219 GeV are averaged based on the luminosities. The BFs of the subparticle (K_S^0, π^0, η and η') decays are not included. Uncertainties are statistical only.

Tag mode	$M_{\rm tag}$ (GeV/c^2)	(I) $N_{\rm tag}^{\rm ST}$	(I) $\epsilon_{\rm tag}^{\rm ST}(\%)$	(II) $N_{\rm tag}^{\rm ST}$	(II) $\epsilon_{\rm tag}^{\rm ST}(\%)$	(III) $N_{\rm tag}^{\rm ST}$	(III) $\epsilon_{\rm tag}^{\rm ST}(\%)$
$D_s^- \to K_S^0 K^-$	[1.948, 1.991]	31941 ± 312	47.36 ± 0.07	18559 ± 261	47.26 ± 0.09	6582 ± 160	46.37 ± 0.16
$D_s^- \to K^+ K^- \pi^-$	[1.950, 1.986]	137240 ± 614	39.47 ± 0.03	81286 ± 505	39.32 ± 0.04	28439 ± 327	38.38 ± 0.07
$D_s^- \to K_S^0 K^- \pi^0$	[1.946, 1.987]	11385 ± 529	16.12 ± 0.11	6832 ± 457	15.71 ± 0.16	2227 ± 220	15.93 ± 0.29
$D_s^- \to K^+ K^- \pi^- \pi^0$	[1.947, 1.982]	39306 ± 799	10.50 ± 0.03	23311 ± 659	10.58 ± 0.05	7785 ± 453	10.39 ± 0.08
$D_s^- \to K_S^0 K^- \pi^- \pi^+$	[1.958, 1.980]	8093 ± 326	20.40 ± 0.12	5269 ± 282	20.19 ± 0.17	1662 ± 217	19.50 ± 0.31
$D_s^- \to K_S^0 K^+ \pi^- \pi^-$	[1.953, 1.983]	15719 ± 289	21.83 ± 0.06	8948 ± 231	21.63 ± 0.09	3263 ± 172	21.29 ± 0.15
$D_s^- \to \pi^- \pi^- \pi^+$	[1.952, 1.982]	37977 ± 859	51.43 ± 0.15	21909 ± 776	50.35 ± 0.22	7511 ± 393	49.32 ± 0.41
$D_s^- \to \pi^- \eta_{\gamma\gamma}$	[1.930, 2.000]	17940 ± 403	43.58 ± 0.15	10025 ± 339	43.00 ± 0.22	3725 ± 252	41.83 ± 0.41
$D_s^- \to \pi^- \pi^0 \eta$	[1.920, 2.000]	42618 ± 1397	18.09 ± 0.11	26067 ± 1196	18.40 ± 0.16	10513 ± 1920	17.69 ± 0.30
$D_s^- \to \pi^- \eta'_{\pi^+\pi^-\eta_{\gamma\gamma}}$	[1.940, 1.996]	7759 ± 141	19.12 ± 0.06	4428 ± 111	19.00 ± 0.08	1648 ± 74	18.56 ± 0.13
$D_s^- \to \pi^- \eta'_{\gamma\rho^0}$	[1.939, 1.992]	20610 ± 538	26.28 ± 0.10	11937 ± 480	26.09 ± 0.14	3813 ± 335	25.94 ± 0.27
$D_s^- \to K^- \pi^+ \pi^-$	[1.953, 1.986]	17423 ± 666	47.46 ± 0.22	10175 ± 448	47.19 ± 0.32	4984 ± 458	45.66 ± 0.59

and those with $0.86 < |\cos\theta| < 0.92$ (end cap) must deposit more than 50 MeV, where θ is the polar angle with respect to the z direction (the positive direction of the MDC axis). To exclude showers that originate from charged tracks, the angle between the position of each shower in the EMC and the closest extrapolated charged track must be greater than 10 degrees. The π^0 (η) candidates are reconstructed through $\pi^0 \to \gamma\gamma$ ($\eta \to \gamma\gamma$) decays, with at least one barrel photon. The diphoton invariant masses for the identification of π^0 and η decays are required to be in the ranges of $[0.115, 0.150]$ GeV/c^2 and $[0.500, 0.570]$ GeV/c^2, respectively. The χ^2 of the kinematic fit constraining $M_{\gamma\gamma}$ to the π^0 or η known mass [10] is required to be less than 30.

Charged particle candidates reconstructed using the information of the MDC must satisfy $|\cos\theta| < 0.93$ with the distance of closest approach to the interaction point (IP) less than 10 cm in the z direction and less than 1 cm in the plane perpendicular to z. Particle identification (PID) of charged kaons and pions is implemented by combining the information of dE/dx from the MDC and the time of flight from the TOF system. For charged kaon (pion) candidates, the likelihood for the kaon (pion) hypothesis is required to be larger than that for a pion (kaon). Electron PID uses EMC information along with dE/dx and time of flight to construct likelihoods for electron, pion, and kaon hypotheses ($\mathcal{L}_e$, $\mathcal{L}_\pi$, and $\mathcal{L}_K$). Electron candidates must satisfy $\mathcal{L}_e/(\mathcal{L}_e + \mathcal{L}_\pi + \mathcal{L}_K) > 0.8$. Additionally, the energy deposited in the EMC by the electron candidate must be more than 80% of the track momentum measured by the MDC.

Candidate K_S^0 mesons are reconstructed with pairs of two oppositely charged particles, whose distances of closest approach to the IP along z are less than 20 cm. These two particles are assumed to be pions without PID applied. Primary and secondary vertices are reconstructed, and the decay length between the two vertices is required to be greater than twice its uncertainty. This requirement is not applied for the $D_s^- \to K_S^0 K^-$ decay due to the low combinatorial background. Candidate K_S^0 mesons are required to have the χ^2 of the vertex fit less than 100 and be inside an invariant-mass window $[0.487, 0.511]$ GeV/c^2, which is about three times the resolution. The invariant mass of the $\pi^+\pi^-$ pair of the $D_s^- \to K^-\pi^+\pi^-$ decay is required to be outside of the K_S^0 invariant mass window to prevent an event being doubly counted in selecting the $D_s^- \to K_S^0 K^-$ and $D_s^- \to K^-\pi^+\pi^-$ tag modes. The ρ^0 candidates are selected via the process $\rho^0 \to \pi^+\pi^-$ with an invariant mass window $[0.620, 0.920]$ GeV/c^2, which is about two times the ρ^0 width. The η' candidates are formed from $\pi^+\pi^-\eta$ and $\gamma\rho^0$ combinations with invariant masses falling within the range of $[0.946, 0.970]$ GeV/c^2, about three times the resolution.

In order to identify the process $e^+e^- \to D_s^{*\pm} D_s^\mp$, the signal windows, listed in Table I, are applied to the recoiling mass ($M_{\rm rec}$) of the tag candidate. The definition of $M_{\rm rec}c^2$ is

$$\sqrt{\left(E_{\rm cm} - \sqrt{c^2|\vec{p}_{\rm tag}|^2 + c^4 m_{D_s}^2}\right)^2 - c^2|\vec{p}_{\rm tag}|^2}, \qquad (5)$$

where $E_{\rm cm}$ is the energy of the e^+e^- CM system, $(\sqrt{|\vec{p}_{\rm tag}|^2 + c^2 m_{D_s}^2}, \vec{p}_{\rm tag}) \equiv p_{\rm tag}$ is the measured four-momentum of the tag candidate, and m_{D_s} is the known

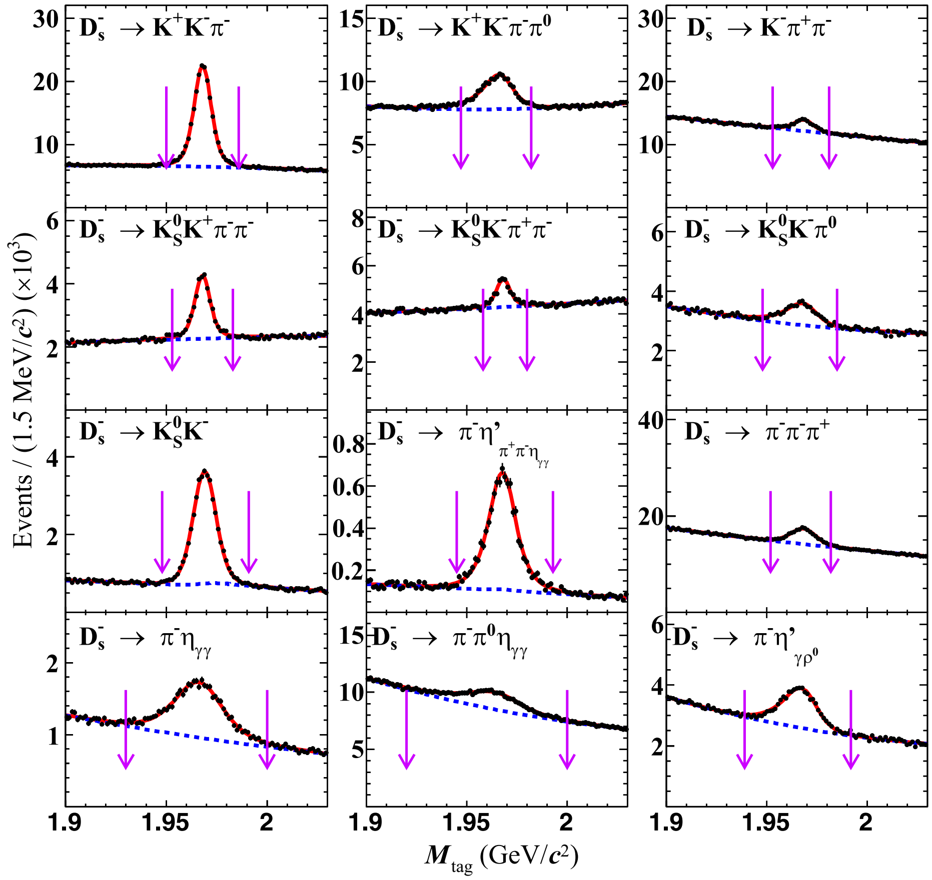

FIG. 3. Fits to the $M_{\rm tag}$ distributions of the ST D_s^- candidates at $\sqrt{s} = 4.178$ GeV. The points with error bars are data, red solid lines are total fits, and blue dashed lines are the fitted backgrounds. The pairs of pink arrows denote signal regions. The peaking background MC-simulated shapes of $D^- \to K_S^0\pi^-$ and $D_s^- \to \eta\pi^+\pi^-\pi^-$ decays are added to the background polynomials in the fits of $D_s^- \to K_S^0 K^-$ and $D_s^- \to \pi^-\eta'$ decays to account for the peaking background, respectively.

D_s^- mass [10]. If there are multiple candidates for a tag mode, the one with $M_{\rm rec}$ closest to the known $D_s^{*\pm}$ mass [10] is chosen.

The ST yields for various tag modes $N_{\rm tag}^{\rm ST}$ are obtained by fitting the $M_{\rm tag}$ distributions of the accepted ST D_s^- candidates. Example fits to the data sample at 4.178 GeV are shown in Fig. 3. The description of the signal shape is based on the MC-simulated shape convolved with a Gaussian function accounting for the resolution difference between data and MC. The background is described by a second-order Chebyshev polynomial. The only two significant peaking backgrounds in all the tag modes are from $D^- \to K_S^0\pi^-$ and $D_s^- \to \eta\pi^+\pi^-\pi^-$ decays faking the $D_s^- \to K_S^0 K^-$ and $D_s^- \to \pi^-\eta'$ tag modes, respectively. The $D^- \to K_S^0\pi^-$ and $D_s^- \to \eta\pi^+\pi^-\pi^-$ background contributions are estimated to be 1724 ± 34 and 89 ± 5 events according to the BFs given by Refs. [10,21], which correspond to about 0.3% and less than 0.1% of the total ST yields, respectively. For these cases, the sizes and MC-simulated shapes of the two peaking backgrounds are fixed based on their BFs and added to the background polynomials. The ST yields in data and ST efficiencies for various tag modes are listed in Table II.

After a D_s^- tag candidate is identified, we search for the signal $D_s^+ \to \pi^0 e^+\nu_e$ candidate recoiling against the tag by requiring one charged particle identified as e^+, one π^0 candidate, and at least one more photon to reconstruct the transition photon of $D_s^{*\pm} \to \gamma D_s^\pm$. Events having charged tracks other than those accounted for in the tagged D_s^- and the electron are rejected. A kinematic fit is performed under the hypothesis $e^+e^- \to D_s^{*\pm}D_s^\mp \to \gamma D_s^+ D_s^-$, with D_s^- decaying to one of the tag modes and D_s^+ decaying to the signal mode. The combination with the minimum χ^2 assuming a D_s^{*+} meson decays to $D_s^+\gamma$ or a D_s^{*-} meson decays to $D_s^-\gamma$ is chosen. The total four-momentum is constrained to the four-momentum of the initial e^+e^- beams. Invariant masses of the tag D_s^-, the signal D_s^+, the D_s^*, and π^0 are constrained to the corresponding known masses [10]. This gives us a total of eight constraints (8C). The missing neutrino four-vector needs to be determined (−4C), so we are left with a four-constraint fit (4C). Furthermore, we require that the maximum energy of

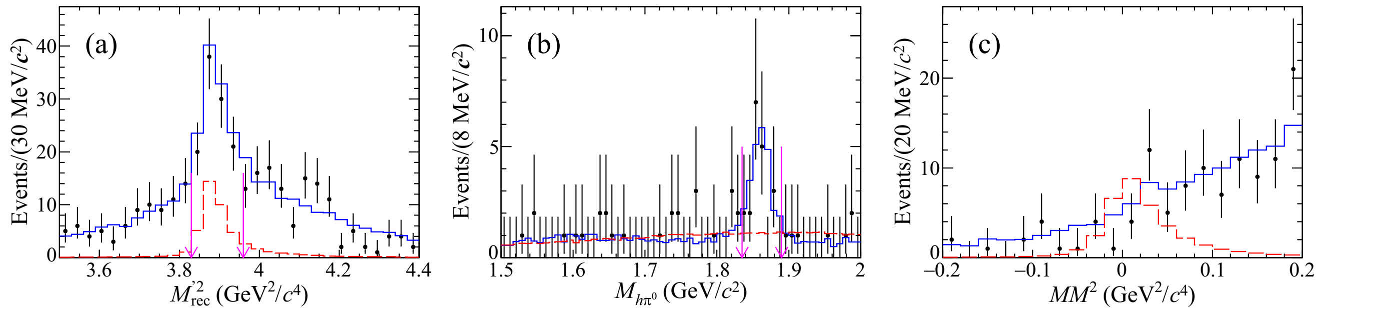

FIG. 4. (a) $M'^2_{\rm rec}$, (b) $M_{h\pi^0}$, and (c) MM^2 distributions of data and MC samples. The points with error bars are data. The blue solid and red dashed lines are inclusive and signal MC samples, respectively. The pair of pink arrows denote the signal windows for (a) and the veto region for (b). The signal MC sample is normalized arbitrarily for visualization purposes. An additional requirement of $|MM^2| < 0.20$ GeV$^2/c^4$ has been applied.

photons not used in the DT event selection is less than 0.2 GeV. The square of the recoil mass against the transition photon and the tag D_s^- ($M'^2_{\rm rec}$) is expected to peak at the known $D_s^\pm$ meson mass squared before the kinematic fit for signal $D_s^{*\pm}D_s^\mp$ events. Therefore, we require $M'^2_{\rm rec}$ to satisfy $3.83 < M'^2_{\rm rec} < 3.96$ GeV$^2/c^4$, as shown in Fig. 4(a). Studies of the inclusive MC sample show that there is a large background coming from $D^0 \to K^- e^+ \nu$ decays versus a hadronic $\bar{D}^0$ decay with a π^0 meson in the final state, where the K^- and the π^0 mesons are interchanged between the two decays. In other words, $D^0 \to K^- e^+ \nu$ versus $\bar{D}^0 \to h\pi^0$ could fake $D_s^+ \to \pi^0 e^+ \nu$ versus $D_s^- \to K^- h$, where h denotes one or more mesons. To suppress this background, for D_s^- tag modes with a K^-, the invariant mass of the π^0 in the reconstructed signal D_s^+ and all the final-state particles of the reconstructed tag D_s^- except the K^- is calculated, called $M_{h\pi^0}$. A veto $1.835 < M_{h\pi^0} < 1.890$ GeV$/c^2$ is applied as shown in Fig. 4(b). This veto removes more than 90% of this background (about 20% of the total background) and sacrifices only about 4% efficiency. The DT efficiencies are obtained using the signal MC samples and listed in Table III.

The missing mass squared of the neutrino is defined as

$$MM^2 = \frac{1}{c^2}(p_{\rm cm} - p_{\rm tag} - p_{\pi^0} - p_e - p_\gamma)^2, \qquad (6)$$

where $p_{\rm cm}$ is the four-momentum of the e^+e^- CM system, and p_i ($i = \pi^0, e, \gamma$) is the four-momentum of the final-state particle i on the signal side. The MM^2 distribution of accepted candidate events is shown in Fig. 4(c). Unbinned maximum-likelihood fits to the MM^2 distribution are performed, where the signal and background shapes are modeled by MC-simulated shapes obtained from the signal and inclusive MC samples, respectively. The fit result is shown in Fig. 5, and the fitted signal yield is -6.9 ± 7.2. Since no significant signal is observed, an upper limit is determined with the likelihood distribution, shown in

TABLE III. DT efficiencies ($\epsilon^{\rm DT}_{\rm tag,sig}$) at $\sqrt{s} =$ (I) 4.178 GeV, (II) 4.189–4.219 GeV, and (III) 4.226 GeV. The efficiencies for the energy points 4.189–4.219 GeV are averaged based on the luminosities. The BF of the π^0 decay is not included. Uncertainties are statistical only.

Tag mode	(I) $\epsilon^{\rm DT}_{\rm tag,sig}(\%)$	(II) $\epsilon^{\rm DT}_{\rm tag,sig}(\%)$	(III) $\epsilon^{\rm DT}_{\rm tag,sig}(\%)$
$D_s^- \to K^+K^-\pi^-$	13.94 ± 0.11	13.18 ± 0.06	12.20 ± 0.11
$D_s^- \to K_S^0 K^-$	10.31 ± 0.04	9.77 ± 0.02	9.02 ± 0.04
$D_s^- \to K_S^0 K^-\pi^0$	4.78 ± 0.07	4.56 ± 0.03	4.34 ± 0.06
$D_s^- \to K^+K^-\pi^-\pi^0$	2.89 ± 0.02	2.79 ± 0.01	2.66 ± 0.02
$D_s^- \to K_S^0 K^-\pi^+\pi^-$	5.38 ± 0.09	5.03 ± 0.04	4.71 ± 0.08
$D_s^- \to K_S^0 K^+\pi^-\pi^-$	5.40 ± 0.07	5.15 ± 0.03	4.84 ± 0.06
$D_s^- \to \pi^+\pi^-\pi^-$	16.92 ± 0.12	15.79 ± 0.06	14.51 ± 0.12
$D_s^- \to \pi^-\eta$	13.98 ± 0.14	13.02 ± 0.07	12.02 ± 0.13
$D_s^- \to \pi^-\pi^0\eta$	6.52 ± 0.04	6.07 ± 0.02	5.52 ± 0.04
$D_s^- \to \pi^-\eta'_{\pi^+\pi^-\eta}$	5.60 ± 0.09	5.31 ± 0.04	4.87 ± 0.09
$D_s^- \to \pi^-\eta'_{\gamma\rho^0}$	7.89 ± 0.08	7.59 ± 0.04	7.05 ± 0.08
$D_s^- \to K^-\pi^+\pi^-$	13.33 ± 0.14	12.51 ± 0.07	11.51 ± 0.13

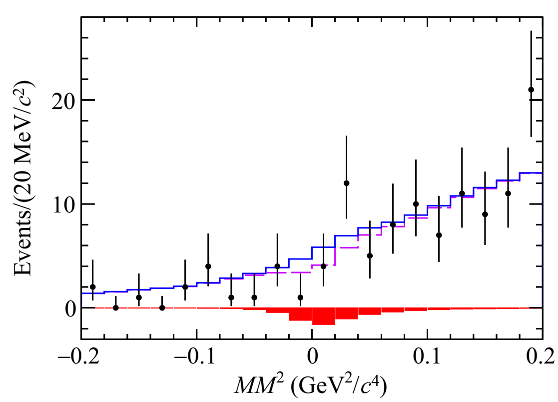

FIG. 5. Fit to MM^2 distribution of data samples. The data are represented by points with error bars, the total fit result by the violet dashed line, the background by the blue solid line, and signal by the red filled histogram.

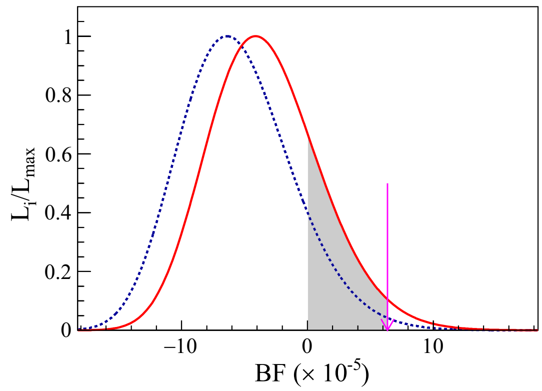

FIG. 6. Likelihood distributions versus BF of the data samples. The likelihood of each bin is denoted as L_i and the maximum of the likelihood is L_{max}. The results obtained with and without incorporating the systematic uncertainties are shown with red solid and blue dashed curves, respectively. The pink arrow shows the result corresponding to the 90% confidence level.

Fig. 6, as a function of assumed BFs. The upper limit on the BF at the 90% confidence level, obtained by integrating from zero to 90% of the resulting curve, is $\mathcal{B}(D_s^+ \to \pi^0 e^+ \nu_e) < 6.4 \times 10^{-5}$. The method to incorporate systematic uncertainty is discussed in the next section.

IV. SYSTEMATIC UNCERTAINTY

The likelihood distribution used in the upper limit measurement covers a range of BFs, as shown in Fig. 6 (or signal events yields). The sources of systematic uncertainties on the BF measurement are classified into two types: additive (or independent of the measured BF central value) and multiplicative (proportional to the BF). The multiplicative ones are summarized in Table IV. Note that most systematic uncertainties on the tag side cancel due to the DT technique.

TABLE IV. Multiplicative systematic uncertainties. All the uncertainties are relative and given in %.

Source	σ_ϵ (%)
D_s^- yield	0.5
$\mathcal{B}(D_s^* \to \gamma D_s)$	0.7
e^+ tracking efficiency	1.0
e^+ PID efficiency	1.0
γ and π^0 reconstruction	3.0
Energy of extra photon	0.5
No extra track	0.9
MC statistics	0.5
Kinematic fit	0.8
Signal model	0.9
Tag bias	0.4
Total	3.9

Additive uncertainties affect the signal yield determination, which is dominated by the imperfect background shape description. This systematic uncertainty is studied by altering the nominal MC background shape with two methods. First, alternative MC samples are used to determine the background shape, where the relative fractions of backgrounds from $q\bar{q}$ and non-$D_s^{*+}D_s^-$ open-charm are varied within their uncertainties, and the BFs of the major $D_s^* D_s$ background sources, i.e., $D_s^+ \to \eta e^+ \nu_e$, $D_s^+ \to f_0 e^+ \nu_e$, $D_s^+ \to K_S^0 e^+ \nu_e$, and $D_s^+ \to \tau^+ \nu_e$, are varied by their listed uncertainties [10]. Second, the background shape is obtained from the inclusive MC samples using a Kernel estimation method [22] implemented in RooFit [23]. The smoothing parameter of RooKeysPdf is varied between 0 and 2 to obtain alternative background shapes. An alternative signal shape based on the simple pole model [24] is tested, but the associated uncertainty is negligible.

Multiplicative uncertainties are from the efficiency determination and the quoted BFs. The uncertainties in the total number of the ST D_s^- mesons is assigned to be 0.5% by examining the changes of the fit yields when varying the signal shape, background shape, and taking into account the background fluctuation in the fit. The uncertainty from the BFs of $D_s^* \to \gamma D_s$ and $\pi^0 \to \gamma\gamma$ decays are 0.7% and 0.03%, respectively, according to the known values [10]. The systematic uncertainty related to e^+ tracking or PID efficiency is assigned as 1.0% from studies of a control sample of radiative Bhabha events. The systematic uncertainties associated with reconstruction efficiencies of the transition photon and π^0 are studied by using control samples of the decay $J/\psi \to \pi^+\pi^-\pi^0$ and the process $e^+e^- \to K^+K^-\pi^+\pi^-\pi^0$, respectively. The efficiency difference between data and MC samples is then determined to be 1.0% for the transition photon and 2.0% for the final state π^0. The uncertainties due to the maximum energy of photons not used in the DT event selection criteria and requiring one charged track are assigned as 0.5% and 0.9%, respectively. We determine these uncertainties by analyzing DT hadronic events in which one D_s^- decays into one of the tag modes and the other D_s^- decays into $K^+K^-\pi^-$ or $K_S^0 K^-$. The uncertainty due to the limited MC sample size is obtained by $\sqrt{\sum_\alpha (f_\alpha \frac{\delta_{\epsilon_\alpha}}{\epsilon_\alpha})^2} \approx 0.5\%$, where f_α is the tag yield fraction, and ϵ_α and δ_{ϵ_α} are the signal efficiency and the corresponding uncertainty of tag mode α, respectively. The acceptance efficiencies of the kinematic fit requirement are studied with the control sample $D_s^+ \to \pi^+\pi^0\eta$ from the DT hadronic $D_s^- D_s^{*+}$ + c.c. events due to its similar topology and large BF. We take into account the difference of the acceptance between data and MC simulation and the statistical uncertainty of this control sample and assign 0.8% as the corresponding uncertainty. We test an alternative simple pole model in place of the ISGW2 model in generating the signal MC sample for the determination of detection efficiency. The form factor of simple pole model is defined as $f_+^{q^2} = \frac{1}{1-\frac{q^2}{M_{\rm pole}}}$, where q is the four-momentum transfer and the pole mass $M_{\rm pole}$ is the known D_s^* mass [10]. The difference of the signal efficiencies between the two models is assigned as the systematic uncertainties related to the MC model. The uncertainty associated with the ST efficiency in Eq. (4) is not canceled fully, which results in a so called "tag bias" uncertainty. We first calculate the difference of ST efficiencies using signal MC and inclusive MC samples, which represents the ST efficiency uncanceled for each tag mode, and then multiply this difference by the systematic uncertainty of the final-state particles reconstruction of the tag mode. The combined results of all tag modes, 0.4%, is assigned as the tag bias uncertainty. The BF of $\pi^0 \to \gamma\gamma$ is $(98.823 \pm 0.034)\%$ [10], which causes a negligible uncertainty, 0.03%.

By adding these uncertainties in quadrature, the total multiplicative systematic uncertainty σ_ϵ is estimated to be 3.9%.

To take into account the additive systematic uncertainty, the maximum-likelihood fits are repeated using different alternative background shapes as mentioned in the previous section and the one resulting in the most conservative upper limit is chosen. Finally, the multiplicative systematic uncertainty σ_ϵ is incorporated in the calculation of the upper limit via [25,26]

$$L(\mathcal{B}) \propto \int_0^1 L\left(\mathcal{B}\frac{\epsilon}{\epsilon_0}\right) \exp\left[\frac{-(\epsilon/\epsilon_0 - 1)^2}{2(\sigma_\epsilon)^2}\right] d\epsilon, \qquad (7)$$

where $L(\mathcal{B})$ is the likelihood distribution as a function of assumed BFs; ϵ is the expected efficiency, and ϵ_0 is the averaged MC-estimated efficiency. The likelihood distributions with and without incorporating the systematic uncertainties are shown in Fig. 6.

V. CONCLUSION

Using a data sample corresponding to an integrated luminosity of 6.32 fb^{-1}, taken at $\sqrt{s} = 4.178$–4.226 GeV recorded by the BESIII detector, we perform the first search for $D_s^+ \to \pi^0 e^+ \nu_e$. No significant signal of the semileptonic decay $D_s^+ \to \pi^0 e^+ \nu_e$ is observed. We set an upper limit on $\mathcal{B}(D_s^+ \to \pi^0 e^+ \nu_e) < 6.4 \times 10^{-5}$ at the 90% confidence level. Our result is consistent with the predicted BF of $D_s^+ \to \pi^0 e^+ \nu_e$, $(2.65 \pm 0.38) \times 10^{-5}$ [1], based on the mechanism of $\pi^0 - \eta$ mixing.

ACKNOWLEDGMENTS

The BESIII collaboration thanks the staff of BEPCII and the IHEP computing center for their strong support. This work is supported in part by National Key Research and Development Program of China under Contracts Nos. 2020YFA0406400, 2020YFA0406300; National Natural Science Foundation of China (NSFC) under Contracts Nos. 11625523, 11635010, 11735014, 11822506, 11835012, 11875054, 11935015, 11935016, 11935018, 11961141012, 12192260, 12192261, 12192262, 12192263, 12192264, 12192265; the Chinese Academy of Sciences (CAS) Large-Scale Scientific Facility Program; Joint Large-Scale Scientific Facility Funds of the NSFC and CAS under Contracts Nos. U2032104, U1732263, U1832207; CAS Key Research Program of Frontier Sciences under Contracts Nos. QYZDJ-SSW-SLH003, QYZDJ-SSW-SLH040; 100 Talents Program of CAS; INPAC and Shanghai Key Laboratory for Particle Physics and Cosmology; ERC under Contract No. 758462; European Union Horizon 2020 research and innovation programme under Contract No. Marie Sklodowska-Curie Grant agreement No. 894790; German Research Foundation DFG under Contracts Nos. 443159800, Collaborative Research Center CRC 1044, FOR 2359, GRK 2149; Istituto Nazionale di Fisica Nucleare, Italy; Ministry of Development of Turkey under Contract No. DPT2006K-120470; National Science and Technology fund; Olle Engkvist Foundation under Contract No. 200-0605; STFC (United Kingdom); The Knut and Alice Wallenberg Foundation (Sweden) under Contract No. 2016.0157; The Royal Society, UK under Contracts Nos. DH140054, DH160214; The Swedish Research Council; U.S. Department of Energy under Contracts Nos. DE-FG02-05ER41374, DE-SC-0012069.

[1] H. B. Li and M. Z. Yang, Phys. Lett. B **811**, 135879 (2020).
[2] S. Gardner, H. B. O'Connell, and A. W. Thomas, Phys. Rev. Lett. **80**, 1834 (1998).
[3] M. Gronau and J. L. Rosner, Phys. Rev. D **79**, 074006 (2009).
[4] G. Ricciardi, Phys. Rev. D **86**, 117505 (2012).
[5] M. Ablikim *et al.* (BESIII Collaboration), Nucl. Instrum. Methods Phys. Res., Sect. A **614**, 345 (2010).
[6] M. Ablikim *et al.* (BESIII Collaboration), Chin. Phys. C **44**, 040001 (2020).
[7] C. H. Yu *et al.*, in *Proceedings of IPAC2016, Busan, Korea* (2016), 10.18429/JACoW-IPAC2016-TUYA01.
[8] X. Li *et al.*, Radiat. Detect. Technol. Methods **1**, 13 (2017); Y. X. Guo *et al.*, Radiat. Detect. Technol. Methods **1**, 15 (2017); P. Cao *et al.*, Nucl. Instrum. Methods Phys. Res., Sect. A **953**, 163053 (2020).

[9] D. Cronin-Hennessy *et al.* (CLEO Collaboration), Phys. Rev. D **80**, 072001 (2009).
[10] P. A. Zyla *et al.* (Particle Data Group), Prog. Theor. Exp. Phys. **2020**, 083C01 (2020) and 2021 update.
[11] M. Ablikim *et al.* (BESIII Collaboration), arXiv:2203.03133.
[12] M. Ablikim *et al.* (BESIII Collaboration), Chin. Phys. C **40**, 063001 (2016).
[13] S. Agostinelli *et al.* (GEANT4 Collaboration), Nucl. Instrum. Methods Phys. Res., Sect. A **506**, 250 (2003).
[14] S. Jadach, B. F. L. Ward, and Z. Was, Phys. Rev. D **63**, 113009 (2001).
[15] D. J. Lange, Nucl. Instrum. Methods Phys. Res., Sect. A **462**, 152 (2001); Ping Rong-Gang, Chin. Phys. C **32**, 599 (2008).
[16] J. C. Chen, G. S. Huang, X. R. Qi, D. H. Zhang, and Y. S. Zhu, Phys. Rev. D **62**, 034003 (2000); R. L. Yang, R.-G. Ping, and H. Chen, Chin. Phys. Lett. **31**, 061301 (2014).
[17] E. Richter-Was, Phys. Lett. B **303**, 163 (1993).
[18] N. Isgur, D. Scora, B. Grinstein, and M. B. Wise, Phys. Rev. D **39**, 799 (1989).
[19] D. Scora and N. Isgur, Phys. Rev. D **52**, 2783 (1995).
[20] J. Adler *et al.* (MARK-III Collaboration), Phys. Rev. Lett. **62**, 1821 (1989).
[21] M. Ablikim *et al.* (BESIII Collaboration), Phys. Rev. D **104**, L071101 (2021).
[22] K. S. Cranmer, Comput. Phys. Commun. **136**, 198 (2001).
[23] R. Brun and F. Rademakers, Nucl. Instrum. Methods Phys. Res., Sect. A **389**, 81 (1997).
[24] T. Becher and R. J. Hill, Phys. Lett. B **633**, 61 (2006).
[25] K. Stenson, arXiv:physics/0605236.
[26] X. X. Liu, X. R. Lyu, and Y. S. Zhu, Chin. Phys. C **39**, 103001 (2015).